Monthly Notices of the ROYAL ASTRONOMICAL SOCIETY

MNRAS **545,** 1–9 (2026) https://doi.org/10.1093/mnras/staf2003
Advance Access publication 2025 November 13

Stellar populations in satellite galaxies in close pairs

A. E. Sansom [1]★ I. Ferreras [2,3,4] and B. F. McDonald[1]

[1]*Jeremiah Horrocks Institute, University of Lancashire, Preston PR1 2HE, UK*
[2]*Instituto de Astrofísica de Canarias, vía Láctea, E-38205 La Laguna, Tenerife, Spain*
[3]*Department of Physics and Astronomy, University College London, London WC1E 6BT, UK*
[4]*Departamento de Astrofísica, Universidad de La Laguna, E-38206 La Laguna, Tenerife, Spain*

Accepted 2025 November 7. Received 2025 October 23; in original form 2025 July 24

ABSTRACT

Satellite galaxies that are near to massive primary galaxies in close pairs can have stellar population ages that are more similar to their primaries than expected. This is one way in which close pairs of galaxies show galactic conformity, which is thought to be driven by assembly bias. Such conformity is seen in ages, morphologies, and star formation rates in different samples. This paper revisits a high signal-to-noise Sloan Digital Sky Survey (SDSS) spectroscopic sample, by spectral fitting of new stellar population models, to investigate satellite galaxy properties of age, metallicity, and α-element abundance. We find the clear signature of age conformity, as previously seen, but no clear evidence for conformity in metallicity or abundance ratios. The offsets showing age conformity are not caused by age–metallicity degeneracies. There is a suggestion in these data that lower velocity dispersion satellites have increased [α/Fe] compared to a control sample of passive galaxies, however this needs further observations to be verified. Our results also suggest an intriguing turnover in the age trends of the satellites at the highest velocity dispersion, perhaps reflecting the onset of environment-related processes in the most massive groups.

Key words: galaxies: abundances – galaxies: evolution – galaxies: formation – galaxies: interactions – galaxies: stellar content.

1 INTRODUCTION

Environmental impacts on galaxy evolution have been extensively investigated, in a range of ways and with various findings (e.g. M. R. Blanton & J. Moustakas 2009; Y.-J. Peng et al. 2010; L. Kawinwanichakij et al. 2017). Environmental effects seem particularly important in the local Universe and less so out to larger redshifts (e.g. B. Darvish et al. 2016; Z. Sattari et al. 2023). One way to study such effects in the local Universe is to look at galaxies in groups, using either the most massive galaxy, referred to as the primary galaxy in a group, or the group halo mass as proxies for the environment of other galaxies in those groups (S. M. Weinmann et al. 2006; A. Pasquali 2015; I. Ferreras et al. 2017). Primaries are often the central and brightest galaxies within a group, although that is not always the case (R. A. Skibba et al. 2011). Such studies have revealed environmental effects often referred to as 'galactic conformity'. Satellite galaxies are seen to be more similar to their more massive primary galaxies in their morphologies (e.g. J. A. Otter et al. 2020); star formation (e.g. J. A. Otter et al. 2020; V. Mesa et al. 2021, and references therein) and in the ages of their stellar populations (F. La Barbera et al. 2014). These studies show that satellites are more quenched than the general population of galaxies at a given stellar mass.

To study this effect in stellar populations I. Ferreras et al. (2019a) created a sample of stacked Sloan Digital Sky Survey (SDSS) DR14 (B. Abolfathi et al. 2018) archive spectra, for satellite galaxies around primary galaxies of different masses. They used stellar velocity dispersion (σ) as an indicator of the local driver for global galaxy characteristics including their star formation histories, because it is known to correlate well with other galaxy parameters (B. Rogers et al. 2010; I. Ferreras et al. 2019b, 2025). Stellar population models from G. Bruzual & S. Charlot (2003) and A. Vazdekis et al. (2012) were fitted to those stacks, using Lick spectral indices (G. Worthey 1998), leading to estimates of relative ages and metallicities. From that work I. Ferreras et al. (2019a) found a significant tendency for satellite galaxies around more massive primaries to be older than those around less massive primaries, for a given satellite velocity dispersion. This age difference was particularly evident for satellite galaxies at lower velocity dispersion.

Single Stellar Population (SSP) models, defined as a model of a stellar population with a single age, metallicity, and abundance pattern [α/Fe], can be used to characterize and compare average properties of galaxies in different sub-sets (e.g. A. Vazdekis et al. 2015). Average α-element to iron-peak abundance ratios from integrated light spectra depend on the duration of star formation in a galaxy (see e.g. G. Worthey, S. M. Faber & J. J. Gonzalez 1992; F. Matteucci & S. Recchi 2001; I. Ferreras & J. Silk 2002; D. Thomas et al. 2005; I. Martín-Navarro et al. 2018). This dependence makes [α/Fe] a useful additional indicator of the star formation history in a galaxy, besides average age measurements. In this work, we apply new semi-empirical SSP models (A. T. Knowles et al. 2023) that sample a range in [α/Fe] to study both age and elemental composition variations within the I. Ferreras et al. (2019a) satellites.

The structure for this paper is as follows. Section 2 describes the galaxy sample used. Section 3 presents details of the spectral fitting and SSP templates used. Section 4 shows the findings from these fits,

★ E-mail: AESansom@lancashire.ac.uk

which are then discussed in Section 5. Finally Section 6 presents our conclusions and discusses future directions.

2 SDSS SAMPLE

SDSS data are well suited to investigate the stellar populations of galaxies with different stellar masses because of the quality, number, and mass range of galaxies with good signal-to-noise spectra. A number of studies with stacked SDSS spectra have indicated effects of environment in the nearby Universe, especially for low and highest mass galaxies (e.g. B. Rogers et al. 2010; F. La Barbera et al. 2014). The data used in this work are based on the sample of satellite galaxy spectra compiled by I. Ferreras et al. (2019a). Full details are given in that paper, however here we summarize the main points. Satellite and primary galaxies were first selected from SDSS DR14 in the redshift range $0.07 < z < 0.14$, with average signal-to-noise ratio per spectral pixel of S/N > 10 in the r band. Primaries have stellar masses $M_* > 10^{11}\mathrm{M}_\odot$ with nearby satellites within a projected distance of $\Delta r_\perp \leq 100$ kpc and redshift offsets corresponding to relative velocities within $|\Delta v_\parallel| \leq 700\,\mathrm{km\,s^{-1}}$ of their primaries. The ratio of satellite mass to primary mass was evaluated for each satellite $\mu = M_{\rm SAT}/M_{\rm PRI}$. The satellites were stacked into five bins in stellar velocity dispersion covering $100 < \sigma < 250\,\mathrm{kms^{-1}}$ and three bins in mass ratio, μ. Error arrays are generated from the error in the mean in each spectral pixel, for each stack. These restrictions in redshift, signal to noise, and velocity dispersion were all aimed at making the selection as unbiased as possible, whilst keeping enough galaxies to maintain a high signal-to-noise ratio (S/N $\gtrsim$ 100 around 5000 Å) when stacked. This work improves on the previous methodology by implementing an algorithm that removes bad individual pixels from the spectra. After masking out bad pixels from each spectrum, we perform a linear interpolation on to a reference (rest frame) wavelength interval $\lambda \in$[3750,7000] Å in log-λ steps of 10^{-4}, when the wavelength is measured in Angstrom. Here, we make use of all five bins in velocity dispersion, but concentrate on only the lowest and highest mass ratio bins, namely $0.158 < \mu_3 < 0.324$ and $0.527 < \mu_1 < 1.000$, respectively. Thus, at fixed velocity dispersion, μ_3 represents satellites around more massive primaries, with respect to μ_1. As a control sample, we also produce a set of stacks in the same selection of five bins in velocity dispersion, but including all SDSS galaxy spectra with the same constraint on S/N. The control sample stacks are contrasted with the satellite spectra to assess the significance of the difference between the μ_1 and μ_3 stacks at fixed velocity dispersion.

Fig. 1 shows an example of the stacks, corresponding to $130 < \sigma < 160\,\mathrm{km\,s^{-1}}$. The top panel shows the ratio between either the μ_1 stack or the μ_3 stack with respect to the control sample. Note the excess flux in the near ultraviolet (NUV) of the control sample with respect to either μ_1 or μ_3. A more subtle difference is found between the two close pairs, so that μ_1 shows a shallower wavelength dependence of this flux ratio. The middle and bottom panels show the S/N and the effective spectral resolution, respectively. The S/N is derived from the error in the mean in each spectral bin of every stack. The characteristic variation in S/N and resolution is evident as the data shifts from the blue to the red arm of the SDSS spectrograph. We note that the stacks are studied at their respective spectral resolution, measured by the code PPXF (M. Cappellari 2017), listed in Table 1. We use the standard MILES (Medium-resolution Isaac Newton Telescope Library of Empirical Spectra) spectral models (A. Vazdekis et al. 2010) for the PPXF fits, although we do not aim at this stage to produce population parameters, leaving that to the next section, where more detailed models are adopted.

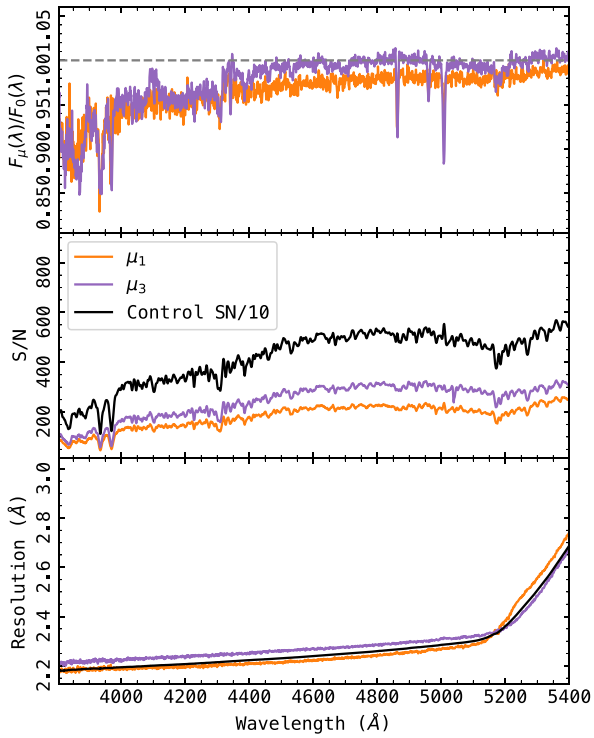

Figure 1. We show some details of the stacks corresponding to the second velocity dispersion bin (σ_2). The top panel shows the ratio between the close pairs stack (μ_1 or μ_3) and the corresponding control stack. The middle panel shows the S/N as a function of wavelength, and the bottom panel corresponds to the effective spectral resolution. The characteristic transition in resolution from the blue to the red arm of the SDSS spectrograph is evident (S. A. Smee et al. 2013).

As a first estimate of the difference in the stellar population content in these stacks, we show in Fig. 2 three typical line strengths as a function of σ. From top to bottom, the figure shows $\mathrm{D}_n(4000)$; $\mathrm{H}\delta_A$; and [MgFe]′. $\mathrm{D}_n(4000)$ is defined as the ratio of fluxes from 100 Å-wide bands either side of the 4000Å break (M. L. Balogh et al. 1999). $\mathrm{H}\delta_A$ is the strength of the Hδ Balmer absorption in the wider definition of G. Worthey & D. L. Ottaviani (1997), and $[\mathrm{MgFe}]' \equiv \sqrt{Mgb(0.72 \times Fe5270 + 0.58 \times Fe5335)}$ is a composite of three Lick indices designed to minimize the effects of [α/Fe] variations (D. Thomas, C. Maraston & R. Bender 2003). The Balmer line has been corrected for emission, using the best fit from the PPXF run. Moreover, the line strengths in this figure are derived from spectra smoothed to a common velocity dispersion of 250 km s^{-1}. This is produced by convolving the spectra with a Gaussian kernel. PPXF is run once more to confirm that the convolved stacks have the target velocity dispersion, within uncertainties. The figure reveals the typical correlation of these indices with σ, as expected from the well-known age–mass and metallicity–mass relations (e.g. A. Gallazzi et al. 2005). At low σ, the control sample, in black, has lower 4000 Å break strength, lower [MgFe]′, and more positive $\mathrm{H}\delta_A$, characteristic of younger populations. Within the satellite sample, those around more massive primaries (i.e. μ_3, in purple in the figure) appear consistently older (stronger 4000 Å break and less positive $\mathrm{H}\delta_A$), in agreement with our previous work (I. Ferreras et al. 2017, 2019a). At the high S/N of the stacked data, it is also worth noting that there is a turnover in the age-sensitive indices $\mathrm{D}_n(4000)$ and $\mathrm{H}\delta_A$ at $\sigma \gtrsim 200\,\mathrm{km\,s^{-1}}$, where μ_3 stacks feature lower 4000 Å break

Table 1. General properties of the stacks used in the analysis. Each row corresponds to one of the five bins in stellar velocity dispersion. μ_1 and μ_3 represent the two extremes in the stellar mass ratio between satellite and primary. The control sample extends to the whole SDSS Legacy data base. For each choice, we show the number of spectra used in each stack, the median S/N per pixel in the rest-frame interval 5000–5500Å (using the error in the mean), and the velocity dispersion (σ in km s^{-1}) measured by PPXF (M. Cappellari 2017).

Vel. Disp.	Range	μ_1			μ_3			Control		
bin	km s^{-1}	N	S/N	σ	N	S/N	σ	N	S/N	σ
σ_1	100–130	36	101	120.0±2.6	188	229	119.7±1.5	71 593	4383	119.5±1.5
σ_2	130–160	140	215	154.0±1.6	256	291	149.6±1.4	69 379	4947	149.2±1.3
σ_3	160–190	205	286	181.0±1.5	128	219	178.2±1.6	51 734	4768	179.7±1.3
σ_4	190–220	172	287	213.0±1.7	70	168	209.6±2.1	29 165	3960	211.8±1.5
σ_5	220–250	85	223	243.6±2.1	23	100	241.8±2.7	13 973	3052	245.3±1.8

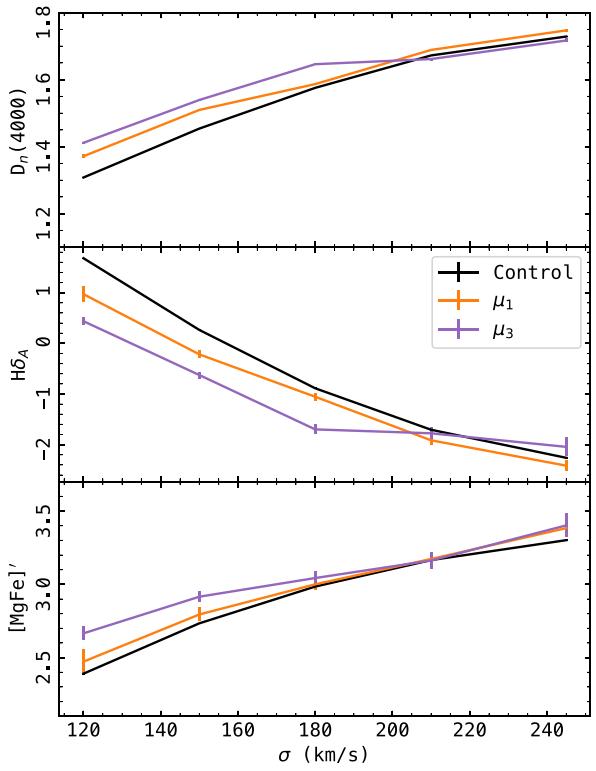

Figure 2. Equivalent widths of the stacks shown as a function of velocity dispersion. From top to bottom we show the 4000 Å break strength, D$_n$(4000), Balmer absorption (Hδ_A), and the [MgFe]′ index. Note the turnover of the age sensitive indices at higher velocity dispersion for the μ_3 stacks. For a consistent comparison, the spectra have been corrected for emission lines and smoothed to a common velocity dispersion of 250 km s^{-1} (see the text for details). Error bars are propagated from the error in the mean of the stacks, shown at the 1 σ level.

strength and Hδ_A, suggestive of a reversal in the age difference in satellites around more (μ_3) or less (μ_1) massive primaries. This is an important issue that will be explored below with models.

3 MEASURING STELLAR POPULATION PARAMETERS

In this work, we look at three stellar population parameters simultaneously. These are light weighted mean stellar population age, metallicity, and [α/Fe] ratio, where the α-element dependence is dominated by magnesium sensitivity in our approach. Fitting all three parameters with SSPs simultaneously becomes possible with our new SSP models that are described below.

3.1 New spectral templates

The new SSP model spectra that we use in this work are from A. T. Knowles et al. (2023) and cover a wide range in ages (0.03 to 14 Gyr), total metallicities ($-1.79 \leq$ [M/H] $\leq +0.26$ dex[1] and also five steps in [α/Fe] of –0.2, 0.0, +0.2, +0.4, and +0.6 abundance ratio. Most previous models only covered two steps in [α/Fe] for the full spectrum (e.g. A. Vazdekis et al. 2015). These new models are built from semi-empirical stars made by combining empirical MILES library stars[2] with modifications from theoretical star spectra[3] that have variable abundances of α-capture to iron peak elements. These SSP models and the semi-empirical stars from which they were made are described in detail in A. T. Knowles et al. (2023, 2021). The theoretical star spectra that went into making the semi-empirical star spectra have α-elements O, Ne, Mg, Si, S, Ca, and Ti all varying together both in the photospheres and in the radiative transfer modelling of individual stars. All other elements were varied together scaled to iron. This means that the [α/Fe] ratios were handled self-consistently throughout the generation of theoretical star spectra. Thus there was no need to assume that the α-elements group were behaving only as trace elements (as is assumed by C. Conroy et al. 2018). This self-consistency of approach propagates through to the SSPs, at the expense of being able to follow multiple elements individually (e.g. as in C. Conroy et al. 2018). Evidence from stars in our own Galaxy (e.g. T. Bensby, S. Feltzing & M. S. Oey 2014; D. H. Weinberg et al. 2019) indicates that the α-elements vary approximately as a group, although there are some known smaller systematic differences. For example, for low metallicity disc stars in our Galaxy [O/Fe] is more enhanced than [Mg/Fe], which in turn is more enhanced than heavier α-capture elements such as Si, Ca, Ti (e.g. see T. Bensby et al. 2014 their fig. 15; A. Hourihane et al. 2023 their fig. 23).

3.2 SSP fitting methodology

To investigate stellar populations in satellite galaxies and how they might be influenced by their location near to primaries, we look at how the satellite galaxy populations compare in their light weighted mean ages, metallicities, and [α/Fe] ratios, at a given satellite velocity dispersion, for the low and high mass ratio categories described above. PYTHON software was written to use the new SSP libraries

[1]Labelled as $[M/H]_{SSP}$ in A. T. Knowles et al. 2023.
[2]https://research.iac.es/proyecto/miles/
[3]https://data.lancashire.ac.uk/178/

Table 2. Stellar population parameters for best fits (minimizing χ^2_ν) to emission-line subtracted stacks of SDSS satellite galaxy spectra, by fitting 15 Lick indices (see Section 3.2). The first column shows the velocity dispersion (σ) bin range being measured. The second column indicates which data set is being measured, in term of mass ratio $\mu = M_{\rm SAT}/M_{\rm PRI}$, or Control sample. The third, fourth, and fifth columns give the best fitting age, metallicity, and [α/Fe] values together with their lower and upper ranges from flux density perturbation error analysis (see Section 3.2). The best fit $\chi^2_\nu/\sqrt{N_g}$ is given, where N_g is the number of galaxies in the stack (see Appendix A for details). For each σ bin, there are four rows: Row 1 gives results for those satellites that have a similar mass to their nearby primaries (μ_1); Row 2 gives results for those satellites that are much less massive (μ_3) than their primaries; Row 3 gives results for the Control sample. Row 4 gives the difference between μ_3 and μ_1 parameters. Recall that all primaries considered in this work are massive ($M_* > 10^{11}{\rm M}_\odot$), as detailed in Section 2.

Vel. Disp. bin	Mass ratio bin	Age (Gyr)	[M/H]$_{\rm SSP}$ (dex)	[α/Fe] (dex)	$\chi^2_\nu/\sqrt{N_g}$
σ_1	μ_1	2.346 (2.255 to 2.453)	−0.003 (−0.030 to 0.024)	+0.264 (0.231 to 0.294)	1.53
	μ_3	2.748 (2.678 to 2.750)	+0.022 (0.013 to 0.034)	+0.216 (0.200 to 0.225)	1.05
	Control	2.103 (2.102 to 2.106)	−0.018 (−0.019 to −0.017)	+0.248 (0.248 to 0.250)	
	$\Delta = \mu_3 - \mu_1$	0.402	0.025	−0.048	
σ_2	μ_1	3.571 (3.500 to 3.699)	+0.055 (0.041 to 0.060)	+0.208 (0.197 to 0.227)	1.28
	μ_3	5.000 (4.877 to 5.000)	+0.032 (0.027 to 0.056)	+0.175 (0.166 to 0.188)	1.26
	Control	3.143 (2.887 to 3.146)	+0.043 (0.042 to 0.072)	+0.198 (0.192 to 0.198)	
	$\Delta = \mu_3 - \mu_1$	1.429	−0.023	−0.033	
σ_3	μ_1	5.598 (5.500 to 5.768)	+0.053 (0.040 to 0.060)	+0.175 (0.167 to 0.183)	1.52
	μ_3	7.395 (7.203 to 7.685)	+0.051 (0.034 to 0.060)	+0.187 (0.179 to 0.197)	1.23
	Control	5.392 (5.371 to 5.406)	+0.055 (0.054 to 0.057)	+0.195 (0.194 to 0.195)	
	$\Delta = \mu_3 - \mu_1$	1.797	−0.002	0.012	
σ_4	μ_1	8.286 (8.113 to 8.435)	+0.060 (0.056 to 0.065)	+0.225 (0.214 to 0.235)	1.82
	μ_3	8.979 (8.698 to 9.336)	+0.019 (0.001 to 0.038)	+0.245 (0.231 to 0.264)	1.22
	Control	7.879 (7.868 to 7.902)	+0.056 (0.055 to 0.057)	+0.202 (0.202 to 0.203)	
	$\Delta = \mu_3 - \mu_1$	0.693	−0.041	0.020	
σ_5	μ_1	10.729 (10.17 to 11.15)	+0.070 (0.060 to 0.082)	+0.239 (0.225 to 0.252)	1.84
	μ_3	8.921 (8.428 to 9.427)	+0.118 (0.091 to 0.147)	+0.232 (0.204 to 0.259)	1.02
	Control	9.034 (9.009 to 9.064)	+0.084 (0.083 to 0.085)	+0.222 (0.221 to 0.223)	
	$\Delta = \mu_3 - \mu_1$	−1.808	0.048	−0.007	

of A. T. Knowles et al. (2023) to search for best fitting SSPs and uncertainties in their three parameters. This SSP fitting software is described in A. T. Knowles et al. (2023). In this work, 15 Lick line indices in the optical range are fitted, to spectra at fixed σ for each stack, by blurring SSP spectra to the central velocity dispersion of each galaxy stack. The Lick line indices included are: H$\delta_{A\&F}$, G4300, H$\gamma_{A\&F}$, Fe4383, Ca4455, Fe4531, Hβ, Mgb, Fe5270, Fe5335, Fe5406, Fe5709, and Fe5782 (defined in G. Worthey & D. L. Ottaviani 1997; S. C. Trager et al. 1998). Amongst these indices the sensitivity to α-elements is mainly through the magnesium sensitivity of Mgb. Hence our fits are more sensitive to [Mg/Fe] than global [α/Fe] changes. We use Lick indices, rather than full spectrum fitting, to include the spectral features that are most sensitive to the stellar population parameters that we aim to measure. This is important because there appear to be some problems in fitting full spectra with α-enhancement (E. Pernet, A. Boecker & I. Martín-Navarro 2024). In this work a fixed bimodal initial mass function (comparable to P. Kroupa 2001) is assumed, which is reasonable given the lack of sensitivity to the stellar initial mass function for galaxies with velocity dispersions below ~ 250 km s^{-1} (E. Pernet et al. 2024, see their fig. 4).

To derive error estimates for the three stellar population parameters, Monte Carlo tests are used, varying the spectral fluxes in the satellite stacks by their uncertainties, Gaussian sampled assuming the Gaussian 1σ is the uncertainty in each spectral bin of the stacks.

3.3 Application to SDSS satellite galaxy stacks

Fitting SSPs to galaxy populations is a useful, controlled way of looking at *relative* behaviours in derived average population parameters (e.g. D. Thomas et al. 2005; F. La Barbera et al. 2013; E. Pernet et al. 2024), without introducing many free parameters. However, galaxy spectra are more complex than this and models are imperfect, therefore the spectral fits to high S/N spectra are imperfect, and hence we note that absolute values in derived average population parameters are less certain. In this work, we concentrate on looking at relative behaviours between satellite galaxies in different environments, focusing on SSP-equivalent results.

We fit the stacks initially and then use those initially fit SSP models to investigate if there is any residual emission line flux in the galaxy spectra. This revealed some weak excess flux (<3 per cent) at the expected locations of some emission lines that could affect the indices being measured. Therefore, we isolate residual emission lines over small wavelength ranges (~ 20 Å) and replace the flux by this initial best fit SSP model, to minimize the effects of line emission in the galaxy spectra. Then fitting is carried out a second time, on these emission line removed spectra, leading to the best fits for light weighted average stellar population parameters from the satellite galaxy stacked spectra. Best fits, errors from perturbations and scaled χ^2_ν values for the best fits are given in Table 2 and parameters are plotted in Fig. 3. The fits are shown in this table for μ_1 and μ_3 stacks and their differences ($\mu_3 - \mu_1$), for the three SSP parameters fitted. The χ^2_ν values only take into account errors in mean spectral values in the stacks and do not account for unknown errors in the model templates or differences between galaxy spectra within a stack. Those additional errors are difficult to quantify. We attempt to consider them by scaling the χ^2_ν values. Therefore, the absolute values derived in these fits are not so reliable, but this work concentrates on looking for relative differences between stacks. This scaling is discussed further in Appendix A.

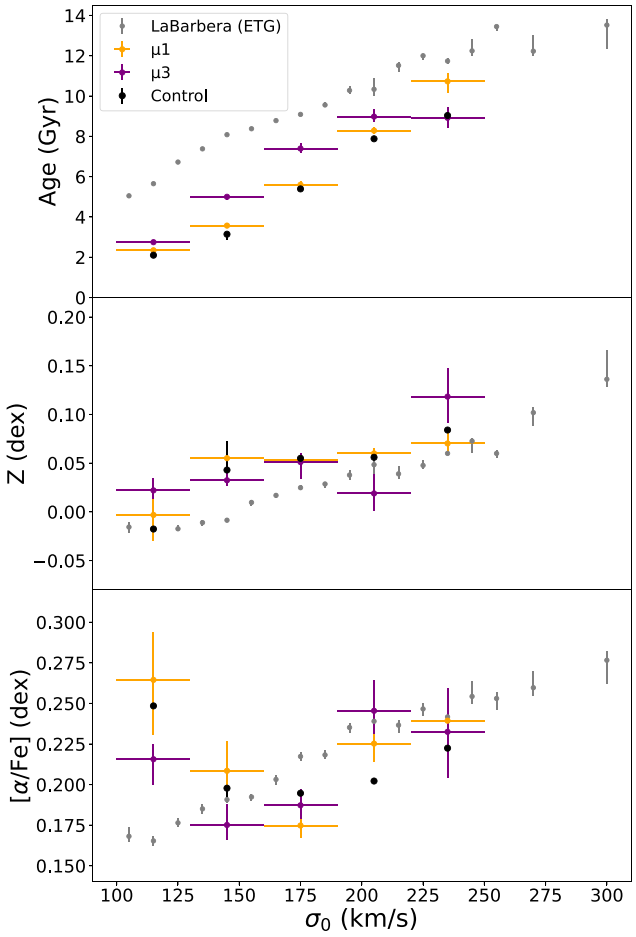

Figure 3. SSP fits to SDSS stacked satellite galaxy data (from I. Ferreras et al. 2019a). Light-weighted ages (top panel), metallicities $Z = [\mathrm{M/H}]_{\mathrm{SSP}}$ (middle panel) and [α/Fe] ratios (lower panel) are given, based on fitting 15 Lick line indices, plotted against stellar velocity dispersion in the middle of each bin (σ_0). Orange points are for satellites with masses just below their nearby primary galaxies (μ_1); purple points are for satellites with much lower masses than their primaries (μ_3); black points are for the control sample without environment constraints; small grey points are from the sample of passive, early-type galaxies (ETG) described in Section 4.1(see the key in the top panel). Uncertainty ranges are obtained from our Monte Carlo perturbations of the spectra being fitted (see Section 3.2).

4 RESULTS

This section describes the results of the SSP fits to stacked spectra of satellite galaxies.

4.1 Full satellite stacks

Using the full satellite stacks described above we measured their stellar population parameters. In Fig. 3, we show how the best fitting parameters compare, for different $\mu = M_{\mathrm{SAT}}/M_{\mathrm{PRI}}$ at the lowest (μ_3) and highest (μ_1) mass ratios, plus in the control sample. Broadly, this figure shows that stellar populations increase in age with increasing velocity dispersion (as is well known from many other studies, e.g. F. La Barbera et al. 2013; R. M. McDermid et al. 2015; I. Ferreras et al. 2019b).

Also plotted in Fig. 3 are the trends that we found in A. T. Knowles et al. (2023) for SDSS data of passive galaxies from F. La Barbera et al. (2013), which we use here as a comparison sample of quiescent galaxies. All points plotted in Fig. 3 are measured in the same way, using our SSP fitting PYTHON code. The grey points of the quiescent sample show age, metallicity, and [α/Fe] all increasing with σ. The ages in our satellites are generally younger than in the quiescent sample but follow a similar slope. Note that our satellite galaxies are not selected to be passive. Metallicities are estimated as slightly higher, and with greater uncertainty in the satellites than in the quiescent sample. There may be some age–metallicity degeneracy systematic affecting the satellites samples, but this is not clear in the trends observed (offsets from the quiescent sample do not anticorrelate). The [α/Fe] values are similar at higher σ, but differ from the quiescent sample in the lowest σ bin.

Whilst age increases with σ for both μ_1 and μ_3 satellite stacks, we see an offset between these two (orange and purple points, respectively). The top panel in Fig. 3 highlights systematic differences in ages of stellar populations, with low mass satellites around massive primaries (μ_3) showing older ages than in satellites with more similar masses to their massive primaries (μ_1) at a given satellite galaxy σ. This difference in stellar population ages, for satellite galaxies with the same σ highlights the impact of their environments, through being close to a primary galaxy. If there was no such environmental influence then there would be no difference between galaxies at the same σ. This is a manifestation of conformity and it agrees qualitatively with what was found in I. Ferreras et al. (2019a). The effect on ages is at the level of up to ~ 2 Gyr difference. The control sample accentuates this difference because it shows younger ages at a given σ than either of the satellite stacks. Note that the satellite stacks show a reversal of behaviour in ages for the highest σ bin, similar to the reversal seen in age-sensitive indices in Fig. 2.

The middle panel in Fig. 3 indicates no significant systematic difference between μ_1 and μ_3 classes of satellite galaxies, at a given σ, hence we do not detect any systematic effect on metallicity of stellar populations in satellite galaxies resulting from proximity to a massive primary galaxy. This lack of systematic difference may indicate that higher signal to noise is needed in the spectra to see such effects, or that light weighted metallicity is less sensitive to environmental impact than light weighted age. Because metallicity is generally determined by redder wavelength features than age, in a composite population, then light-weighted metallicity estimates are more influenced by older stars than are the light-weighted age estimate. Satellites may experience a range of environments through their histories as they are pre-processed in field or group environments before their their current group is formed (M. Oxland et al. 2024 and references therein). Larger scale group and cluster formation occurs later than the formation of galaxies within those groups, therefore the metallicities may be more strongly affected by their histories, whereas ages are more strongly affected by the most recent star formation. Their evolution in these environments will determine their average stellar abundances (e.g. B. Bidaran et al. 2022). These effects, and the uncertainties in measuring metallicities may contribute to why we do not see a systematic effect for metallicity. The control sample is also consistent with metallicity estimates for the satellites.

The lowest panel in Fig. 3 indicates that [α/Fe] values tend to increase towards higher σ, as is observed generally for more massive, passive galaxies (e.g. F. La Barbera et al. 2013; I. Martín-Navarro et al. 2018). However, there is a suggestion of an upturn in [α/Fe] for our lowest σ bin [$\sim 115\,\mathrm{km\ s^{-1}}$, for all samples of our stacks (μ_1, μ_3 and control samples)]. The quiescent sample does not show such an upturn. This upturn needs further investigation in larger samples of galaxies to find out if it is real. Between the μ_3 and μ_1 mass ratio bins there is no evidence for a systematic change in

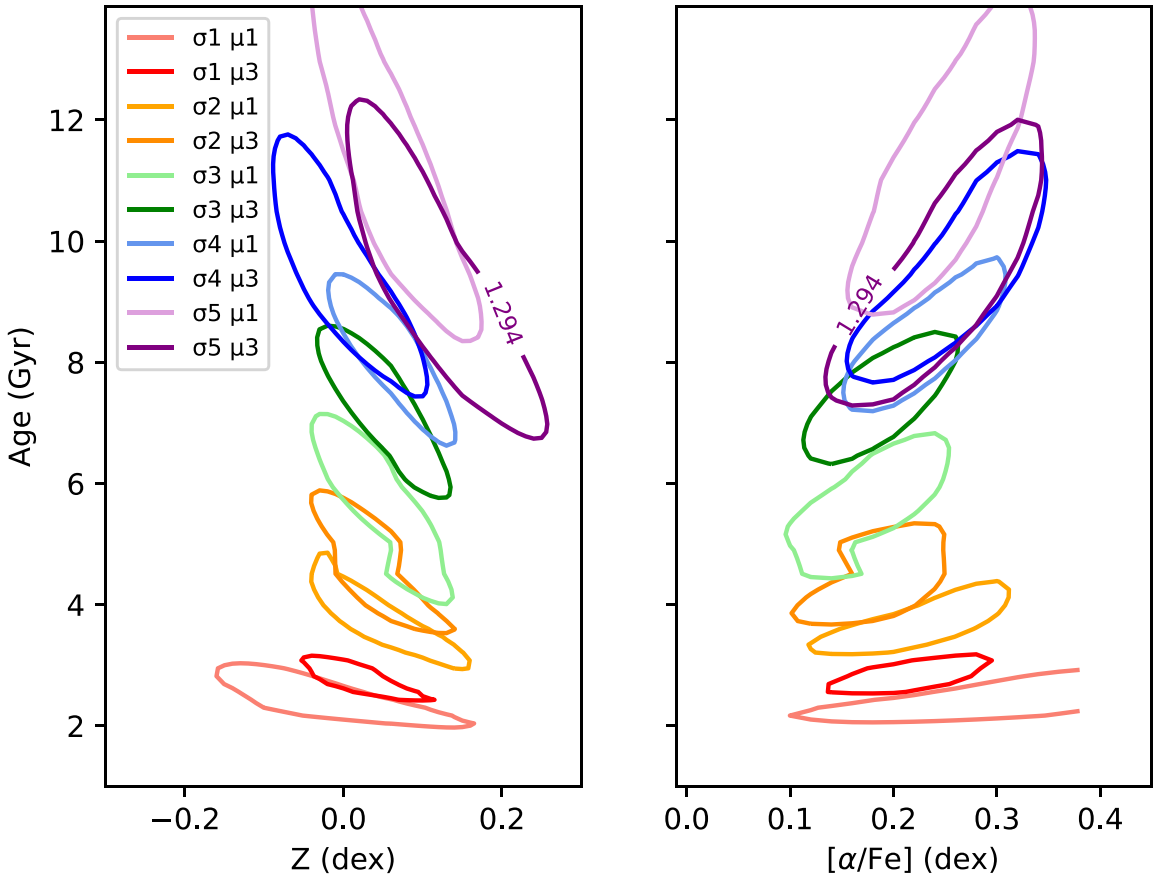

Figure 4. This figure shows normalized χ^2_ν contours for SSP fits to the satellite galaxy stacks at five different stellar velocity dispersions. Contours are plotted at 1σ confidence level for three fitted parameters, fitting 15 Lick indices. Here, σ_1 to σ_5 are the lowest to highest velocity dispersion bins as listed in Table 2. At each σ, satellite stacks with low $M_{\rm SAT}/M_{\rm PRI}$ (μ_3) are shown with a darker contour line and satellite stacks with higher $M_{\rm SAT}/M_{\rm PRI}$ (μ_1) are shown with a lighter contour line. On the left are plotted contours in age and metallicity ($= Z = [{\rm M/H}]_{\rm SSP}$) space, at the best fitting [α/Fe]. On the right are plotted contours in Age and [α/Fe], at the best fitting metallicity.

[α/Fe], at a given σ, and hence no evidence of environment affecting that parameter in satellite galaxies in close pairs with their primary galaxies.

To investigate these trends for correlated effects we plot χ^2_ν contours in two parameters, whilst fixing the third parameter at the best-fitting value. In Fig. 4, we plot χ^2_ν contours from grids of our SSP fits, which are also generated by the PYTHON SSP fitting code. The χ^2_ν values plotted are normalized by the best fitting model χ^2_ν, to account for galaxy-to-galaxy scatter and systematic differences between the models and data. These normalized χ^2_ν contour plots allow us to map the distribution of where the best fits occur and to look at results more independently of the well known age–metallicity degeneracy effect. The contours are plotted at a level of $1.0 + 3.53/(15 - 3) = 1.294$. The value of 3.53 is for 68 per cent confidence with three free parameters (see e.g. W. H. Press et al. 1992) and there are 15 Lick indices being fitted with three parameters.

Fig. 4 (left panel) highlights the systematic difference between μ_3 (darker contours) and μ_1 (lighter contours) satellites in their ages, with μ_1 contours sitting below μ_3 contours, particularly for the lowest σ stacks. Whilst metallicity is not very well constrained the offsets between contours in the vertical (age) axis reveal age differences, with relatively low mass ratio satellites (μ_3) appearing older than higher mass ratio satellites (μ_1). Fig. 4 (right panel) again shows this age offset (vertical axis) but illustrates no significant offset in [α/Fe] (horizontal axis).

4.2 Marginalized results

For the full satellite stacks we plot the contours again but this time marginalizing over the third parameter in each case, as a more stringent test of the offsets. Fig. 5 shows that the age offsets are still present, even when the third parameter (not plotted) is marginalized over. That is, any value of the third parameter is allowed over the input range for that parameter. This equates to collapsing the third parameter axis, rather than fixing the third parameter to its best-fitting value (as was done in Fig. 4).

Thus our finding of age offsets in satellite galaxies of the same σ, due to conformity, remains when we use the new stellar population models with a wide range in [α/Fe] values. This result is independent of any age–metallicity degeneracy effect, as seen in Figs 4 and 5 left panels.

5 DISCUSSION

More massive galaxies tend to have higher velocity dispersions and older stellar populations. The primary galaxies used to characterize the local environments in groups in this study are massive galaxies ($M_* > 10^{11}{\rm M}_\odot$). We found here and in I. Ferreras et al. (2019a, 2017) that ages of satellite galaxies tend to be more similar to that of their primary galaxies in close pairs than expected for the velocity dispersion of the satellites. This is seen as older ages

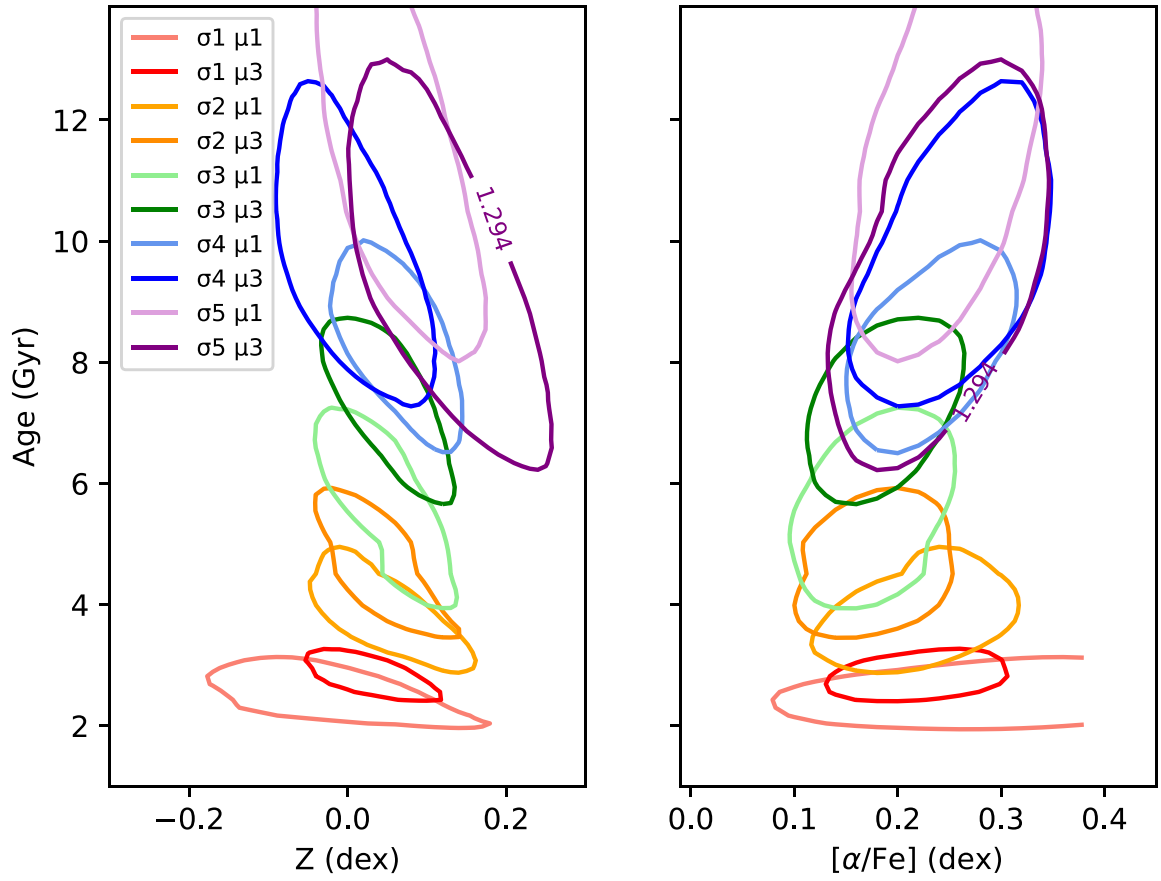

Figure 5. Same as in Fig. 4 but for SSP fits marginalized over the third parameter not plotted in each case.

in satellites with lower masses compared to their primaries, thus conforming more to the primary galaxy properties than expected. If there was no such conformity effect then, at a given σ, satellites would not show such systematic offsets in age (Fig. 5). In this paper, we show that this age offset is still present even when [α/Fe] is allowed to vary. Age conformity may be a result of cessation of star formation being influenced by the environment of a satellite galaxy, including its proximity to a more massive primary galaxy. For example, ram pressure stripping and starvation of interstellar medium gas may be more effective close to a massive primary galaxy in a group. Then without the gas to form new stars the satellite galaxy becomes passive earlier. The light-weighted average age of the satellite will then depend on when it fell into the group, with more recent acquisitions still possessing younger stars.

This work shows no significant offsets in metallicity between our μ_1 and μ_3 satellite stacks. For the metallicity, this may have been determined mainly by the evolution of the satellite in field and groups prior to its infall into the group of the central. This pre-processing could explain why we do not see effects of conformity in the metallicity between satellites and centrals. Whilst there is strong evidence of pre-processing of galaxies from observations (A. Hou, L. C. Parker & W. E. Harris 2014; B. Bidaran et al. 2022) and models (S. L. McGee et al. 2009), the exact effects on element abundances, how that leads to scaling relations and offsets, is not well known. More work is needed to be able to statistically follow how stellar population parameters behave in pre-processing and due to current environment effects.

A well studied possibility is that the primaries and secondaries were made at about the same time, with lower mass ratios (μ_3) surviving in older groups (assembly bias, see discussion in I. Ferreras et al. 2019a and references therein; K. Wang et al. 2022). Assembly bias was revealed and is supported by cosmological simulations (e.g. L. Gao, V. Springel & S. D. M. White 2005; A. D. Montero-Dorta et al. 2021). Is it possible to distinguish between different mechanisms? Changes with redshift or cluster concentration in simulations and comparisons with data may help to distinguish between various scenarios. New data are becoming available in ongoing and future large scale surveys, such as the Dark Energy Spectroscopic Instrument (DESI) survey (DESI Collaboration 2022) or the WHT Enhanced Area Velocity Explorer (WEAVE) stellar population survey (S. Jin et al. 2024).

Finally, we also discuss the turnover of the age trend at the highest velocity dispersion. In Fig. 2, the ordering of the line strengths with respect to the mass ratio, μ, are found to change in the σ_5 bin, a result that is reflected in Fig. 3, so that the μ_3 stacks appear *younger* than μ_1 galaxies, in contrast with all the other stacks at lower velocity dispersion. While the error bars in metallicity and [α/Fe] are larger, it is also worth pointing out that this turnover also suggests μ_3 galaxies in the σ_5 bin having higher metallicity and perhaps lower [α/Fe], although this result is rather weak. This result can be interpreted as an external channel of evolution in close pairs, at the highest velocity dispersion, μ_3 galaxies – that have a very massive primary – potentially the central galaxy of a massive group or cluster. In such pairs, we would expect the satellite to be affected by the well-known environment effects that produce younger ages in central

galaxies of massive groups (e.g. F. La Barbera et al. 2014; A. Pasquali 2015). In contrast, at lower velocity dispersion, the trends are, rather, suggestive of a more generic effect related to assembly bias, instead of the microphysics of galaxy formation in massive groups. This turnover appears to be rather robust, given the consistent trend in such a large number of high quality SDSS spectra. Therefore, we propose it as a useful test of the sub-grid physics in cosmological simulations of galaxy formation (e.g. J. Schaye et al. 2015; A. Pillepich et al. 2018).

6 CONCLUSIONS

We have used new stellar population models (A. T. Knowles et al. 2023), with a wider range of [α/Fe] values than previously available, to simultaneously fit light-weighted ages, metallicities, and [α/Fe] values to stacked SDSS spectra of satellite galaxies in close pairs with primary galaxies. With these new SSP models we confirm the results of I. Ferreras et al. (2019a) that satellites with low mass ratios compared to their primaries are systematically older than satellites with masses more similar to their primaries. Figs 3 and 5 show this systematic offset for four out of five bins in satellite velocity dispersion. Thus we detect evidence of conformity in ages of satellite galaxies, such that they are more like their primaries than expected for their stellar velocity dispersion. A control sample of galaxies, not selected by environment, is slightly younger than either satellite sample at a given σ (Fig. 3), which is expected because they are not generally close to massive galaxies and hence are not so affected by conformity.

In this work, we also looked for evidence of conformity in element abundances. In contrast to ages, we do not detect any systematic effects in the abundances (metallicity or [α/Fe]) between low and high mass ratio satellites. Offsets between these mass ratios do not show systematic effects in Figs 3 or 5. Evidence such as that shown here will help to constrain simulation of hierarchical structure and galaxy formation (e.g. Y.-T. Lin et al. 2022).

Compared to a quiescent sample of passive galaxies (not selected by environment) the satellite galaxies studied here have younger ages (Fig. 3, top panel); similar metallicities (Fig. 3, middle panel), and similar [α/Fe] except in the lowest σ bin (Fig. 3, lowest panel). Results for the high [α/Fe] measurement in satellites in the lowest σ bin need more data to confirm that result.

We also find a robust turnover in the ages of the satellites at the highest velocity dispersion, with μ_3 stacks appearing younger than μ_1 galaxies, a trend that suggests the effect of environment processes in the most massive groups, a result that is potentially a useful test of the baryon physics in numerical simulations.

ACKNOWLEDGEMENTS

A. E. Sansom acknowledges support from the University of Central Lancashire, Jeremiah Horrocks Institute for undergraduate research internship funding for Benjamin McDonald during summer 2023. Funding for SDSS-III has been provided by the Alfred P. Sloan Foundation, the Participating Institutions, the National Science Foundation and the U.S. Department of Energy Office of Science. The SDSS-III web site is https://www.sdss3.org/. Thanks to the referee (Prof. Jon Loveday) for comments that helped to improve this paper.

DATA AVAILABILITY

The semi-empirical SSP libraries used in this work were presented in A. T. Knowles et al. (2023) and are publicly available on the Lancashire Online Research Data repository (https://data.lancashire.ac.uk/388/) and MILES website (http://research.iac.es/proyecto/miles/pages/other-predictionsdata.php).

REFERENCES

Abolfathi B. et al. 2018, ApJS, 235, 42
Balogh M. L., Morris S. L., Yee H. K. C., Carlberg R. G., Ellingson E., 1999, ApJ, 527, 54
Bensby T., Feltzing S., Oey M. S., 2014, A&A, 562, A71
Bidaran B. et al., 2022, MNRAS, 515, 4622
Blanton M. R., Moustakas J., 2009, ARA&A, 47, 159
Bruzual G., Charlot S., 2003, MNRAS, 344, 1000
Cappellari M., 2017, MNRAS, 466, 798
Conroy C., Villaume A., van Dokkum P. G., Lind K., 2018, ApJ, 854, 139
Darvish B., Mobasher B., Sobral D., Rettura A., Scoville N., Faisst A., Capak P., 2016, ApJ, 825, 113
Davis T. A. et al., 2020, MNRAS, 496, 4061
DESI Collaboration, 2022, AJ, 164, 207
Ferreras I. et al., 2017, MNRAS, 468, 607
Ferreras I. et al., 2019b, MNRAS, 489, 608
Ferreras I., Hopkins A. M., Lagos C., Sansom A. E., Scott N., Croom S., Brough S., 2019a, MNRAS, 487, 435
Ferreras I., Silk J., 2002, MNRAS, 336, 1181
Ferreras I., Trevisan M., Lahav O., de Carvalho R. R., Silk J., 2025, MNRAS, 540, 1069
Gallazzi A., Charlot S., Brinchmann J., White S. D. M., Tremonti C. A., 2005, MNRAS, 362, 41
Gao L., Springel V., White S. D. M., 2005, MNRAS, 363, L66
Hou A., Parker L. C., Harris W. E., 2014, MNRAS, 442, 406
Hourihane A. et al., 2023, A&A, 676, A129
Jin S., et al., 2024, MNRAS, 530, 2688
Kawinwanichakij L. et al., 2017, ApJ, 847, 134
Knowles A. T., Sansom A. E., Allende Prieto C., Vazdekis A., 2021, MNRAS, 504, 2286
Knowles A. T., Sansom A. E., Vazdekis A., Allende Prieto C., 2023, MNRAS, 523, 3450
Kroupa P., 2001, MNRAS, 322, 231
La Barbera F., Ferreras I., Vazdekis A., de la Rosa I. G., de Carvalho R. R., Trevisan M., Falcón-Barroso J., Ricciardelli E., 2013, MNRAS, 433, 3017
La Barbera F., Pasquali A., Ferreras I., Gallazzi A., de Carvalho R. R., de la Rosa I. G., 2014, MNRAS, 445, 1977
Lin Y.-T., Miyatake H., Guo H., Chiang Y.-K., Chen K.-F., Lan T.-W., Chang Y.-Y., 2022, A&A, 666, A97
Martín-Navarro I., Vazdekis A., Falcón-Barroso J., La Barbera F., Yıldırım A., van de Ven G., 2018, MNRAS, 475, 3700
Matteucci F., Recchi S., 2001, ApJ, 558, 351
McDermid R. M. et al., 2015, MNRAS, 448, 3484
McGee S. L., Balogh M. L., Bower R. G., Font A. S., McCarthy I. G., 2009, MNRAS, 400, 937
Mesa V., Alonso S., Coldwell G., Lambas D. G., Nilo Castellon J. L., 2021, MNRAS, 501, 1046
Mitzkus M., Cappellari M., Walcher C. J., 2017, MNRAS, 464, 4789
Montero-Dorta A. D., Chaves-Montero J., Artale M. C., Favole G., 2021, MNRAS, 508, 940
Otter J. A., Masters K. L., Simmons B., Lintott C. J., 2020, MNRAS, 492, 2722
Oxland M., Parker L. C., de Carvalho R. R., Sampaio V. M., 2024, MNRAS, 529, 3651
Pasquali A., 2015, Astron. Nachr., 336, 505
Peng Y.-J. et al., 2010, ApJ, 721, 193
Pernet E., Boecker A., Martín-Navarro I., 2024, A&A, 687, L14

Pillepich A. et al., 2018, MNRAS, 473, 4077
Press W. H., Teukolsky S. A., Vetterling W. T., Flannery B. P., 1992, Numerical Recipes in C. The Art of Scientific Computing. Cambridge Univ. Press, Cambridge
Rogers B., Ferreras I., Pasquali A., Bernardi M., Lahav O., Kaviraj S., 2010, MNRAS, 405, 329
Sattari Z. et al., 2023, ApJ, 951, 147
Schaye J. et al., 2015, MNRAS, 446, 521
Skibba R. A., van den Bosch F. C., Yang X., More S., Mo H., Fontanot F., 2011, MNRAS, 410, 417
Smee S. A. et al., 2013, AJ, 146, 32
Thomas D., Maraston C., Bender R., 2003, MNRAS, 339, 897
Thomas D., Maraston C., Bender R., Mendes de Oliveira C., 2005, ApJ, 621, 673
Trager S. C., Worthey G., Faber S. M., Burstein D., González J. J., 1998, ApJS, 116, 1
Vazdekis A. et al., 2015, MNRAS, 449, 1177
Vazdekis A., Ricciardelli E., Cenarro A. J., Rivero-González J. G., Díaz-García L. A., Falcón-Barroso J., 2012, MNRAS, 424, 157
Vazdekis A., Sánchez-Blázquez P., Falcón-Barroso J., Cenarro A. J., Beasley M. A., Cardiel N., Gorgas J., Peletier R. F., 2010, MNRAS, 404, 1639
Wang K., Mao Y.-Y., Zentner A. R., Guo H., Lange J. U., van den Bosch F. C., Mezini L., 2022, MNRAS, 516, 4003
Weinberg D. H. et al., 2019, ApJ, 874, 102
Weinmann S. M., van den Bosch F. C., Yang X., Mo H. J., 2006, MNRAS, 366, 2
Worthey G., 1998, PASP, 110, 888
Worthey G., Faber S. M., Gonzalez J. J., 1992, ApJ, 398, 69
Worthey G., Ottaviani D. L., 1997, ApJS, 111, 377

APPENDIX A: FITTING STATISTIC FOR STACKED DATA

Our analysis of stacked data faces an important issue regarding the absolute value of the best-fitting statistic, i.e. the minimum value of the reduced χ^2 statistic (χ^2_ν). As the number of individual spectra in each stack is fairly high (see Table 1), the associated uncertainty per spectral bin is rather small, and the resulting χ^2_ν is high. However, in the stacking procedure we typically quote the error in the mean, which would be an accurate description if each individual spectra were to represent noisy realizations of the same galaxy. The stacking of different galaxies implies that, in addition to the error in the mean, one should also take into account the scatter among galaxies. We follow an empirical approach to assess this term by plotting the reduced χ^2 with respect to the number of spectra in each bin, N_g (see Fig. A1). Note the clear trend of the data with respect to a $\sqrt{N_g}$ scaling (grey solid line). A least-squares fit (dashed black line) gives a very similar result. Therefore, we adopt the $\sqrt{N_g}$ trend to produce an effective χ^2_ν statistic, as quoted in Table 2. Similar types of scaling have been implemented on the best-fitting statistic in other studies for a more meaningful comparison of the parameters (see e.g. M. Mitzkus, M. Cappellari & C. J. Walcher 2017; T. A. Davis et al. 2020). This scaling does not change the best-fitting SSP parameter values.

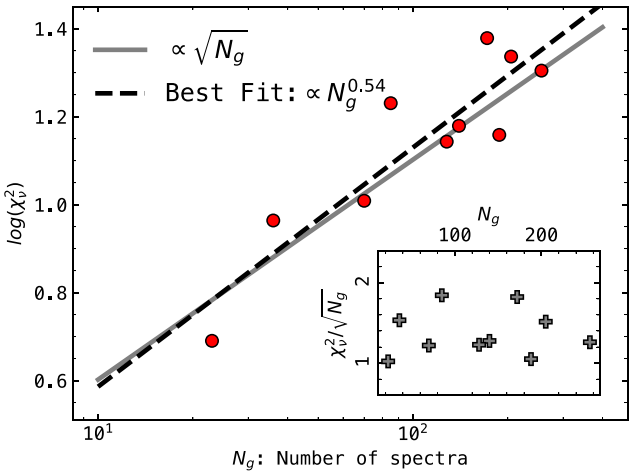

Figure A1. Trend of the reduced χ^2 statistic (χ^2_ν, derived from the error in the mean) for the SSP analysis, shown with respect to the number of spectra in each stack, N_g, along with the best fit (black dashed line), and a simple $N_g^{1/2}$ scaling (grey solid line). The inset shows the effective χ^2_ν after being divided by this scaling factor.

This paper has been typeset from a TEX/LATEX file prepared by the author.